applied sciences

MDPI

Article

Hydraulic Design and CFD-Based Parametric Study for Optimizing Centrifugal Pump Impeller Performance

Abdurashid Aliuly [1,2,*], Tangnur Amanzholov [1,2,*], Abzal Seitov [1,2], Nazerke Momysh [1,2], Nurbolat Jaichibekov [1,3] and Aidarkhan Kaltayev [2]

[1] Joldasbekov Institute of Mechanics and Engineering, Almaty 050010, Kazakhstan; seitov.abzal9@gmail.com (A.S.); nazerke.momysh@gmail.com (N.M.); jaichnur@gmail.com (N.J.)
[2] Department of Mechanical Engineering, Satbayev University, Almaty 050013, Kazakhstan; aidarkhan.kaltayev@gmail.com
[3] Department of Mechanics, L.N. Gumilyov Eurasian National University, Astana 010008, Kazakhstan
* Correspondence: aliuly.abdurashid@gmail.com (A.A.); tannur.amanzholov@gmail.com (T.A.); Tel.: +7-707-135-20-20 (A.A.); +7-707-555-17-35 (T.A.)

Abstract: Centrifugal pumps are extensively utilized across various industries, including water supply, agriculture, and energy, where they consume significant amounts of electricity. As demands for energy efficiency and reduced operating costs increase, enhancing pump efficiency has become crucial. This study focuses on optimizing the pump impeller geometry, which plays a vital role in minimizing energy losses. A hydraulic and hydrodynamic model was developed, alongside a parametric study based on numerical simulations (CFD), to analyze the influence of geometric parameters—specifically the angles and shapes of the blade's inlet and outlet edges—on energy losses and hydraulic efficiency. The study utilized experimental data provided by the manufacturer for model verification. The results revealed that Ivanovsky's method displayed deviations in the blade width at the leading edge and trailing edge of 25% and 43%, respectively, while Spiridonov's method indicated deviations of 13% in the outer diameter D_2 and 27.5% in the blade width at the trailing edge. In contrast, the combined method proposed by the authors achieved high accuracy, with deviations under 9%. Additionally, parametric analysis identified two key parameters affecting the pump efficiency: the angle of the trailing edge and its shape. These findings underscore the necessity of optimizing the blade geometry to enhance the performance and energy efficiency of centrifugal pumps.

Keywords: impeller; centrifugal pump; hydraulic design; CFD simulation; parametric study

Citation: Aliuly, A.; Amanzholov, T.; Seitov, A.; Momysh, N.; Jaichibekov, N.; Kaltayev, A. Hydraulic Design and CFD-Based Parametric Study for Optimizing Centrifugal Pump Impeller Performance. *Appl. Sci.* **2024**, *14*, 10161. https://doi.org/10.3390/app142210161

Academic Editor: Cesare Biserni

Received: 1 October 2024
Revised: 14 October 2024
Accepted: 29 October 2024
Published: 6 November 2024

1. Introduction

Centrifugal pumps are widely used in various sectors, such as water supply and wastewater for drinking water, energy for transferring heat carriers in heat exchangers, industry for transporting industrial liquids and chemical solutions, particularly in oil fields [1–3], as well as in agriculture for field irrigation, etc. In the context of today's pursuit of increased competitiveness, compliance with regulatory requirements [4], and reduction in operational costs [5–7], the task of enhancing the energy efficiency of centrifugal pumps becomes particularly relevant.

The impeller of a centrifugal pump generates centrifugal forces that facilitate the movement of fluid from the center to the periphery, converting the mechanical energy of the rotating blades into the kinetic energy of the flow. However, various energy losses occur during fluid flow through the pump. Frictional forces between the fluid and the blade walls, the shape of the diffuser, and turbulent flow contribute to the formation of vortices, which lead to energy loss [8–10]. Additionally, cavitation phenomena, which occur when the local pressure drops below the saturation vapor pressure, negatively impact the pump's energy efficiency and reliability [11–13]. To enhance the efficiency of centrifugal pumps, a

comprehensive analysis of these factors is required, along with the exploration of ways to minimize them using high-precision methods.

The centrifugal pump system comprises several key components: the inlet pipe, impeller, volute, and outlet extension pipe. A significant portion of energy losses occurs at the impeller, making its geometric parameters particularly crucial for optimizing the pump's performance. While hydraulic calculations can provide optimal parameters, the application of detailed CFD modeling enables a more precise analysis and enhancement of the flow characteristics, ultimately contributing to an increase in the pump's hydraulic efficiency.

One of the main geometric parameters of the impeller is the angles of the leading and trailing edges of the blades, as well as the wrap angles. In the study by X. Han et al. [14], the impact of the wrap angle and the trailing edge angle on the pump's efficiency and head was investigated. The analysis of four parameters, such as the change in static pressure, relative velocity, streamlines, and kinetic energy, showed that at a wrap angle of 126° and a trailing edge angle of 24°, the efficiency value was significantly higher compared to the original parameters. In their studies, A. P. S. Wheeler et al. [15] and H. Luo et al. [16] examined the influence of the leading-edge shape (elliptical, arcuate and circular) on the hydraulic losses in the impeller. They found that blunter and sharper edge shapes cause a flow compression effect, which at high flow rates create a negative velocity gradient at the inlet, leading to energy losses and a localized low-pressure region. The shape of the impeller's trailing edge has also been studied as an optimization parameter, particularly regarding its influence on the backflow and energy losses. Research showed that the shape of the trailing edge has a minimal impact on the impeller's leading section. However, optimizing the trailing edge, specifically by thinning it, significantly reduces the vortices and energy losses, resulting in an improved flow and a 0.59% increase in overall pump efficiency. Conversely, thickening the trailing edge leads to a decrease in the efficiency by approximately 6% [17]. The study [18] examined the impact of modifying the impeller's trailing edge on the efficiency and head of a centrifugal pump at various specific speeds, based on CFD simulations and experiments. The research in [19–21] demonstrated that optimizing the blade thickness in centrifugal pumps significantly affects their performance, efficiency, and durability, highlighting the importance of precise blade design to enhance the operational characteristics of pumps.

Many of the above studies have shown that the use of CFD numerical modeling significantly enhances the effectiveness of pump optimization and serves as a valuable tool for the detailed analysis of flows, vortices, and other parameters. However, the need for further improvement in impeller design remains a pressing challenge. In this regard, the aim of this study is to minimize the losses caused by hydraulic and local resistances to improve the pump's flow characteristics.

To overcome this challenge, a hydraulic calculation model was developed to determine the initial optimal geometric parameters of the impeller and volute of the pump. The study applied numerical modeling methods using Ansys CFX, along with experimental data from an existing centrifugal pump to verify the simulation results. The choice of these methods is justified by their high accuracy and ability to conduct a detailed investigation of the pressure and velocity fields, as well as provide in-depth analysis for optimizing the pump design, ultimately leading to a significant improvement in its energy efficiency.

The results of this study are expected to significantly improve the efficiency (COP) of centrifugal pumps, which in turn will reduce the energy consumption and enhance the reliability of pumping systems. The research enables a more precise identification of the parameters to which the pump efficiency is most sensitive and evaluates their impact on the overall energy efficiency of the pump.

2. Methodology

2.1. Characteristics of the Centrifugal Pump CHP 150-315/1500

This study examines a typical centrifugal pump model CHP 150-315/1500 (Karlskrona LC AB (Shymkent, Kazakhstan)) (Figure 1a), produced at the Karlskrona factory, which

is widely used for pumping various liquids in sectors such as water supply, energy, and industry. The authors of this article have access to experimental data regarding this pump model from the manufacturer. However, since these data are confidential, there are certain restrictions on its publication. Nevertheless, basic information on the performance and key characteristics of the pump has been provided (Table 1), including the main geometric parameters of the impeller (Table 2). These data are considered sufficient for the development of a mathematical model, verification of the results, and further detailed analysis. It is important to note that the verification aims to confirm the accuracy of the developed mathematical models, enabling their use for subsequent design and optimization. Experimental data allow for an assessment of how accurately the models reproduce the actual operating conditions of the pump and its performance.

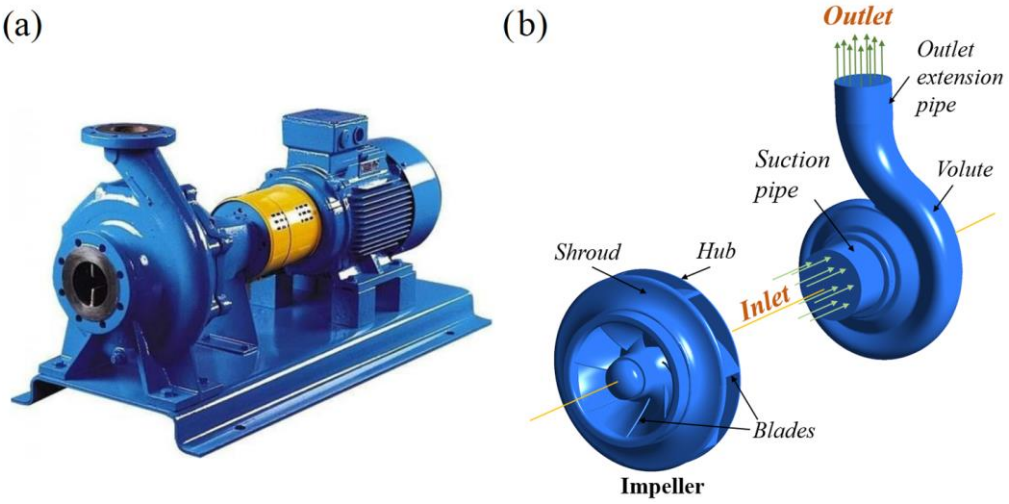

Figure 1. CHP 150-315/1500 pump unit (**a**) and computational domain (**b**).

Table 1. Main characteristic curves.

Q, [m^3/h]	H, [m]	P, [kW]	η, [%]
216.6	33.0	29.40	66.3
270.4	32.1	32.11	73.7
321.8	31.2	36.54	74.9
340.1	30.3	37.32	75.3
358.7	29.4	38.58	74.5
382.2	28.5	41.47	71.5
397.7	27.5	42.37	70.4

Table 2. Impeller geometrical parameters.

Parameters	CHP 150-315/1500
D_{sh}, [mm]	46
D_h, [mm]	60
D_0, [mm]	190
D_1, [mm]	132
D_2, [mm]	324
b_1, [mm]	80
b_2, [mm]	40
β_1, [°]	20
β_2, [°]	34

2.2. Hydraulic Calculations of the Basic Structural Design of a Single-Stage Pump

The actual flow entering the impeller is characterized by complex and uneven features. The flow has a complicated structure and non-uniformity around the circumference and

width of the impeller. Vortex flows are observed in the inter-blade channels and the volute, leading to the emergence of local hydraulic resistances that negatively affect the overall efficiency of the system.

Due to the complex nature of the flow, an analytical solution to the problem is unavailable. Therefore, in practice, calculation methods are applied based on various simplifications and assumptions, where a detailed study of the flow at every point is not required, only at the control sections. As a flow parameter, the actual value is taken as its average integral value over the area of the flow cross section. For such a significantly simplified problem, the theory of one-dimensional homogeneous flows is applicable, where the problem is treated as one-dimensional and depends only on one coordinate, namely the radial vector. The theory based on such assumptions is called the theory of hydraulic machines. To describe the kinematics of the fluid in the theory of hydraulic machines, a velocity triangle or velocity plan is used (Figure 2), where the absolute flow velocity $\vec{c}$ is defined as the sum of the circumferential flow velocity $\vec{u}$ and the relative flow velocity $\vec{w}$ [22], as expressed in Equation (1).

$$\vec{c} = \vec{u} + \vec{w} \tag{1}$$

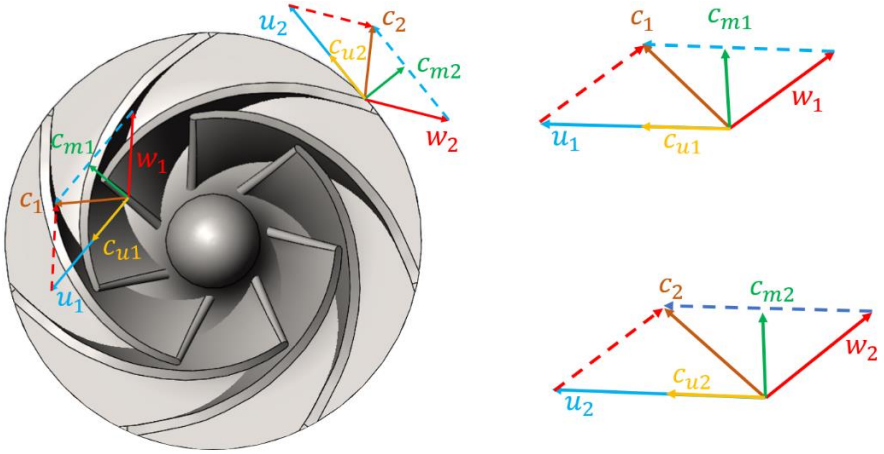

Figure 2. Kinematics of fluid flow in the impeller. Velocity triangles.

This visual representation of velocities allows for a more accurate analysis and optimization of the pump's flow characteristics and its interaction with the blades of the impeller.

Calculation of the Main Geometric Parameters of the Impeller

To calculate the optimal parameters of a centrifugal pump, specifically the impeller, the optimal velocities that ensure the maximum efficiency are first determined. Only after that are the optimal dimensions of the impeller calculated. These key geometric parameters are determined at three different sections of the impeller (Figure 3a): at the impeller entry point (0-0), at the leading edge (LE) of the blade (1-1) and at the trailing edge (TE) of the blade (2-2). The required volumetric flow rate Q, head H, and rotational speed n are specified as input data for the calculation.

The specific speed coefficient plays an important role in pump classification, determining the blade shape, blade inclination angles, and the pump's performance characteristics [23–27], and is defined by Equation (2):

$$n_s = 0.65n\frac{Q^{\frac{1}{2}}}{H^{\frac{3}{4}}}. \tag{2}$$

The efficiency coefficient η of a centrifugal pump is defined as the ratio of useful power to the power received from the motor. As mentioned earlier, due to losses (leakage,

friction, geometry), the pump efficiency decreases. To minimize such losses, three types of efficiency are considered in the hydraulic calculation: volumetric efficiency η_v, which takes into account the leakage and bypasses from seals, as well as the effect of the cavity between the impeller and the volute casing; hydraulic efficiency η_h, which includes the losses related to cavitation, local obstacles, hydraulic friction, vortices, and flow separation from the blades; and mechanical efficiency η_m, which reflects the losses associated with the bearing friction and fluid friction in the cavity between the impeller and the volute. Each efficiency component is determined using the following empirical equations [28].

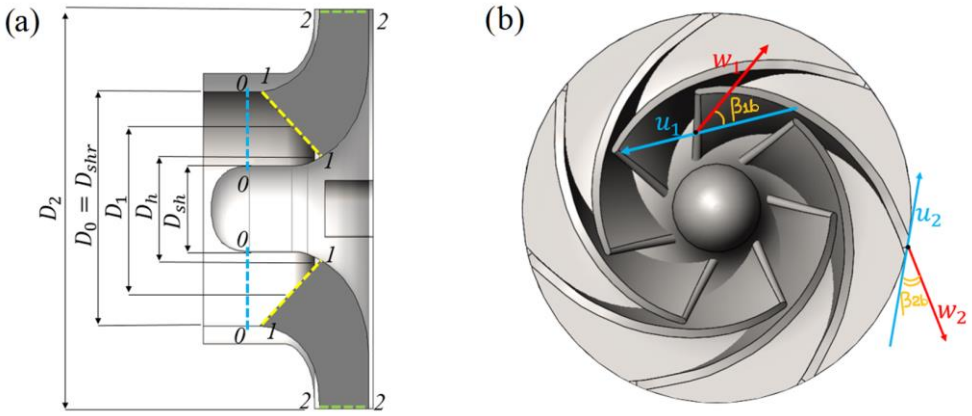

Figure 3. Meridional section (**a**) and plan view (**b**) of the impeller.

$$\eta_v = \frac{1}{1 + 0.68 n_s^{-(2/3)}} \tag{3}$$

$$\eta_h = 1 - \frac{0.42}{\left(\lg D_{1\Pi p} - 0.172\right)^2} \tag{4}$$

$$\eta_m = \frac{1}{1 + 820 {n_s}^{-2}} \tag{5}$$

The preliminary assessment of the overall efficiency of a centrifugal pump is determined by the product of all three efficiencies [25,28] and is calculated using Equation (6):

$$\eta = \eta_v \eta_h \eta_m. \tag{6}$$

The shaft diameter (Figure 3a) is calculated based on strength conditions, taking into account the torques acting on the shaft axis, and is determined by the following equation [25]:

$$D_{sh} = \sqrt[3]{\frac{16\ M}{\pi\ [\tau]}}, \tag{7}$$

where

$$M = \frac{N_{max}}{\omega} = \frac{N_{max}}{2\pi n} \tag{8}$$

$$N_{max} = \frac{\rho g H Q}{1000\ \eta}, \tag{9}$$

where M [Nm]—torque, $[\tau]$—allowable torsional stress, and for carbon steel material $[\tau]$ = 13–15 MPa [26].

According to the strength condition [23], the hub diameter (Figure 3a) must be at least 10% greater than the shaft diameter.

$$D_h = (1.2 \div 1.5) D_{sh} \tag{10}$$

To satisfy this condition, the coefficient in front of D_{sh} in Equation (10) is found to be in the range of 1.2–1.25 in the works of Spiridonov [25] and Mikhailov [27], while in the works of Ivanovsky [24] and Gorgidzhanyan [26], it falls within the ranges of 1.1–1.25 and 1.2–1.4, respectively.

The absolute flow velocity at the inlet to the impeller is determined by Equation (11):

$$c_0 = 0.06\sqrt[3]{Q_{imp}n^2}, \tag{11}$$

where the flow rate of the impeller Q_{imp} is defined as follows [24–26]:

$$Q_{imp} = \frac{Q}{\eta_v}. \tag{12}$$

The diameter of the inlet funnel of the impeller, as shown in Figure 3a at section 0-0, is determined based on the law of mass conservation.

$$D_0 = \sqrt{\frac{4Q_{imp}}{\pi c_0} + {D_h}^2} \tag{13}$$

The average diameter of the LE of the blade (Figure 3a) depends on the type of pump and is defined for low-speed and normal pumps according to Equations (14) and (15), respectively, as stated in the work of [25].

$$D_1 = (0.9 \div 1.1)D_0 \tag{14}$$

$$D_1 = (0.7 \div 0.9)D_0 \tag{15}$$

In Gorgidzhanyan's study [26], the coefficients applied to the diameter D_0 depend on the value of the specific speed n_s. For cases where $n_s \leq 90$, the coefficient ranges from 0.9 to 1.0, whereas for $n_s > 90$, it ranges from 0.6 to 0.9. In this context, lower coefficient values correspond to higher specific speed coefficients.

The meridional flow velocity at the inlet to the blade is determined using the following formula, taking into account the flow constriction caused by the impeller blades:

$$c_{1m} = k_1 c_0\,. \tag{16}$$

The value of the constriction coefficient k_1 in the works of [23,26] ranges between 1.1 and 1.15, while in Mikhailov's work [27] it falls within the range of 1.15 to 1.2. During the calculation, this coefficient is refined until the condition $\left|k_1' - k_1\right| \leq 0.01$ is satisfied, as stated in the works of [24,25]. This condition is similarly applied to the coefficients k_2 and k in subsequent steps.

The width of the impeller blade LE (Figure 3a) is determined by Equation (17):

$$b_1 = \frac{2Q_{imp}}{\pi(D_{sh} + D_h)c_{1m}}. \tag{17}$$

The inclination angle of the LE of the blade (Figure 3b) is determined from the velocity triangle [24,25]:

$$\beta_{1b} = arctg\frac{c_{1m}}{u_1 - c_{1u}} + \Delta\beta_1, \tag{18}$$

where the circumferential component of the absolute flow velocity $c_{1u} = 0$, since the flow at the blade inlet enters without circulation, and the tangential velocity u_1 at the inlet is determined by Equation (19).

$$u_1 = D_1\pi\frac{n}{60} \tag{19}$$

At the inlet, there exists a specific angle of attack $\Delta\beta_1$ between the axial line of the blade and the flow vector. The normal range for this angle is from -2° to 5° [24], while other sources indicate a variation from 3° to 8° [25,26]. The latter sources note that to improve the cavitation reserve, the angle of attack may be increased up to 15°.

The meridional component of the absolute velocity at the TE of the impeller blade can be determined using the following equation [24,25]:

$$c_{2m} = k_2 c_0. \tag{20}$$

The inclination angle of the TE of the impeller blade (Figure 3b) is determined using Equation (21):

$$\beta_{2b} = arcsin\left[\left(\frac{w_1}{w_2}\right)_{opt}\frac{c_{2m}}{c_{1m}}\frac{k_2}{k_1}sin\beta_{1b}\right], \tag{21}$$

where the optimal ratio of relative velocities is defined by the empirical Equation (22).

$$\left(\frac{w_1}{w_2}\right)_{opt} = 5.65 \cdot 10^{-5} n_s^2 - 18.23 \cdot 10^{-3} n_s + 2.65 \tag{22}$$

The circumferential velocity at the TE of blade is expressed by the following equation [24,25]:

$$u_2 = \frac{c_{2m}}{2tg\beta_{2b}} + \sqrt{\left(\frac{c_{2m}}{2tg\beta_{2b}}\right) + gH_{th} + c_{1u}u_1}. \tag{23}$$

The theoretical head is the head without accounting for losses [24,25] and is defined by the following equation:

$$H_{th} = \frac{H}{\eta_h k}. \tag{24}$$

The diameter of the impeller is determined using Euler's equation and is calculated as (Figure 3a):

$$D_2 = \frac{60u_2}{\pi n}. \tag{25}$$

The width of the TE of the impeller blade (Figure 3a) is determined by expression (26):

$$b_2 = \frac{Q_{imp}k_2}{\pi D_2 c_{2m}}. \tag{26}$$

The number of blades on the pump impeller is determined by the following equation [24]:

$$z = A\frac{D_2 + D_1}{D_2 - D_1}\sin\left(\frac{\beta_{1b} + \beta_{2b}}{2}\right). \tag{27}$$

All the calculated data are considered the initial optimal parameters in the design of a centrifugal pump from scratch. For further optimization and improvement of the pump's efficiency, more detailed calculations are performed based on the CFD.

2.3. CFD Modeling

Hydrodynamic modeling using computational fluid dynamics (CFD) methods allows for in-depth investigation of fluid behavior in complex geometries, such as the impeller and volute casing of a centrifugal pump. The use of CFD technologies makes it possible to accurately predict the distribution of the pressure and velocity fields, as well as to evaluate the efficiency of the pump under various operating conditions. This is especially important at the stage of pump design and optimization, as it allows identifying and eliminating potential problems before production.

This part of the paper presents the hydrodynamic modeling of a centrifugal pump using CFD. It includes the stages of the problem formulation and geometry construction,

the generation of a computational grid, the formulation of assumptions, the setting of boundary and initial conditions, and the selection of mathematical models.

2.3.1. Problem Statement and Geometry

The centrifugal pump CHP 150-315/1500 manufactured by Karlskrona LC AB was used for the study. The target parameters of the pump were as follows: pressure H = 32 m, flow Q = 300 m^3/h, rotation speed n = 1500 rpm, and efficiency η = 80%. The geometric parameters of the pump are given in Table 1.

A three-dimensional (3D) model of a centrifugal pump model CHP 150-315/1500 was used for the simulation, as shown in Figure 1b. The suction pipe served to maintain the homogeneity of the flow at the inlet, which ensured the correct formulation of the boundary conditions. To prevent backflow at the outlet of the system, an outlet extension pipe was used, which contributed to the stability of the solution and the accuracy of the simulation.

2.3.2. Mathematical Model

Modeling flows in centrifugal pumps requires careful consideration of complex turbulent phenomena, which play a key role in the formation of the hydrodynamic characteristics of the pump. Models based on the averaged Navier–Stokes equations (RANS) are widely used to describe turbulence in hydrodynamic problems.

RANS models are based on averaging the Navier–Stokes equations, which allows one to take into account the influence of turbulent fluctuations on the flow without having to directly model all scales of turbulence. This is achieved by decomposing instantaneous quantities such as velocity and pressure into average and pulsating components. The averaging process leads to the appearance of additional terms, known as Reynolds stresses, which describe turbulent stresses in the flow:

$$\frac{\partial \rho}{\partial t} + \frac{\partial}{\partial x_j}(\rho U_j) = 0 \tag{28}$$

$$\frac{\partial \rho U_i}{\partial t} + \frac{\partial}{\partial x_j}(\rho U_i U_j) = -\frac{\partial p'}{\partial x_i} + \frac{\partial}{\partial x_j}\left[\mu_{eff}\left(\frac{\partial U_i}{\partial x_j} + \frac{\partial U_j}{\partial x_i}\right)\right] + S_M, \tag{29}$$

where S_M is the sum of body forces and μ_{eff} is the effective viscosity defined by

$$\mu_{eff} = \mu + \mu_t, \tag{30}$$

and p' is a modified pressure, defined by

$$p' = p + \frac{2}{3}\rho k. \tag{31}$$

Modeling flows in centrifugal pumps requires accurate consideration of not only turbulent processes but also the interaction of the flow with the impeller blades and the features of the flow around the pump channels. One of the key turbulence models used to solve such problems is the Shear Stress Transport (SST) model, implemented in the Ansys CFX software package (v.23.2).

The SST model combines the advantages of two widely used turbulence models: the k-ω model, which is effective near the walls, and the k–ε model, which is more suitable for modeling the main part of the flow. Thanks to this approach, the SST allows for more accurate modeling of the flow separation, which often occurs in centrifugal pumps, especially in the area of the impeller blades and volute. One of the important aspects of using the SST model is its ability to take into account the effects of low Reynolds numbers, which is especially important for modeling the boundary layer, which significantly affects

the flow distribution and, therefore, the pump characteristics such as the pressure and efficiency. The turbulent viscosity μ_t in the SST model is calculated as follows [29,30]:

$$\mu_t = \frac{\rho a_1 k}{\max(a_1\omega, SF_2)}, \tag{32}$$

where S is the invariant measure of the strain rate, and F_2 is a second blending function.

The equation for the turbulence kinetic energy is

$$\frac{\partial k}{\partial t} + U_j\frac{\partial k}{\partial x_j} = P_k - \beta^* k\omega + \frac{\partial}{\partial x_j}\left[(\nu + \sigma_\omega \nu_T)\frac{\partial k}{\partial x_j}\right]. \tag{33}$$

The specific dissipation rate is

$$\frac{\partial \omega}{\partial t} + U_j\frac{\partial \omega}{\partial x_j} = \alpha S^2 - \beta\omega^2 + \frac{\partial}{\partial x_j}\left[(\nu + \sigma_\omega \nu_T)\frac{\partial \omega}{\partial x_j}\right] + 2(1 - F_1)\sigma_{\omega 2}\frac{1}{\omega}\frac{\partial k}{\partial x_i}\frac{\partial \omega}{\partial x_i}. \tag{34}$$

The closure coefficients and auxiliary relations [31,32] are

$$F_2 = \tanh\left[\left[\max\left(\frac{2\sqrt{k}}{\beta^*\omega y}, \frac{500\nu}{y^2\omega}\right)\right]^2\right] \tag{35}$$

$$P_k = \min\left(\tau_{ij}\frac{\partial U_i}{\partial x_j}, 10\beta^* k\omega\right) \tag{36}$$

$$F_2 = \tanh\left\{\left\{\min\left[\max\left(\frac{\sqrt{k}}{\beta^*\omega y}, \frac{500\nu}{y^2\omega}\right), \frac{4\sigma_{\omega 2}k}{CD_{k\omega}y^2}\right]\right\}^4\right\} \tag{37}$$

$$CD_{k\omega} = \max\left(2\rho\sigma_{\omega 2}\frac{1}{\omega}\frac{\partial k}{\partial x_i}\frac{\partial \omega}{\partial x_i}, 10^{-10}\right) \tag{38}$$

$$\phi = \phi_1 F_1 + \phi_2(1 - F_2). \tag{39}$$

The constants are

$$\begin{gathered}\alpha_1 = \tfrac{5}{9},\ \alpha_2 = 0.44,\ \beta_1 = \tfrac{3}{40},\ \beta_2 = 0.0828,\ \beta^* = \tfrac{9}{100} \\ \sigma_{k1} = 0.85,\ \sigma_{k2} = 1,\ \sigma_{w1} = 0.5,\ \sigma_{w2} = 0.856.\end{gathered} \tag{40}$$

In the context of the shear stress transport (SST) model, the α_1, β_1, σ_{k1}, and σ_{w1} constants are specifically tailored for the k–ω model, which is effective near the walls. These constants play a key role in determining the turbulent viscosity and the overall behavior of the turbulent flow, especially in regions close to the wall where the effects of turbulence are most pronounced.

On the other hand, the α_2, β_2, σ_{k2}, and σ_{w2} constants are used for the $k-\varepsilon$ model, which is more suitable for modeling the bulk of the flow away from the boundaries. These parameters help to accurately represent the turbulent kinetic energy and its dissipation, which contributes to a more complete understanding of the flow behavior under various conditions.

The SST model effectively combines the strengths of both the k–ω and k–ε models by using the mentioned constants to provide a more accurate representation of the flow, especially in predicting flow separation and other critical phenomena in centrifugal pumps.

The following simplifying assumptions were made when modeling the flow in a centrifugal pump using ANSYS CFX [33]:

- Stationary flow: the fluid flow is considered stationary, i.e., the time variations in the velocity and pressure are not taken into account, which simplifies the solution of the problem and reduces the computational costs.
- Constant fluid properties: the parameters such as viscosity and density are assumed to be constant throughout the flow, eliminating complex thermodynamic processes and simplifying the calculations.
- Incompressible fluid: the fluid is assumed to be incompressible, which eliminates the effect of density changes on the flow and simplifies the solution of the Navier–Stokes equations.
- Smooth walls: to eliminate the effect of roughness on the fluid flow, the pump walls are assumed to be perfectly smooth, which eliminates microscopic defects that could affect the result.
- Constant temperature: the flow is assumed to be isothermal, i.e., without temperature changes, which eliminates the heat transfer and related processes.
- Impeller periodicity: This interface boundary condition is used to model a single blade sector to reduce the computational time and work time.

The high-resolution discretization scheme was employed, which ensures the automatic enhancement of the accuracy in regions with smooth flow variations and increases the stability in areas with steep gradients. The convergence criterion was set using the Residual Type RMS with a target value of 1×10^{-4}. The analysis was conducted under a steady-state approach.

2.3.3. Initial and Boundary Conditions

The mass flow rate of the fluid at the outlet extension pipe was set at 83.33 kg/s as the outlet boundary condition, which corresponds to the main parameters of the pump under investigation. At the inlet boundary in the suction pipe, a boundary condition of 0.3 atm was established, equal to the NPSH value, in order to prevent cavitation. These boundary conditions ensure accurate modeling of the pump's operating regime and prevent the occurrence of undesirable processes such as cavitation (Figure 1b).

When modeling the wall flow, the automatic wall function for the SST model was used in ANSYS CFX. This method adapts between a low-Reynolds number approach and wall functions based on the local mesh resolution and y+ values. This allows for an accurate representation of the near-wall region without the need for excessive boundary layer refinement, ensuring proper modeling of the velocity profile and wall effects.

Interfaces were installed at the joints between the main pump elements: the suction pipe and the impeller, the impeller and the volute, and the volute and the outlet extension pipe. To model the interaction of the rotating impeller with the stationary volute, the boundary conditions of the "frozen rotor" interface were used. This allows taking into account the rotation of the impeller while maintaining the stationarity of the calculations, which optimizes the computational process and ensures accuracy in modeling the hydrodynamic interaction between components.

2.3.4. Calculation Mesh Construction

The ANSYS Meshing module was used to discretize the design domains of the centrifugal pump. Structured meshes were used in the suction and discharge pipe areas to ensure uniform flow. Due to the complex geometry of the impeller and volute and to improve the adaptability of the mesh to flow characteristics, unstructured meshes were used in these areas, as shown in Figure 4.

To ensure proper resolution of the boundary layers, a total of 12 layers were implemented in the mesh near the walls of the blade surfaces. The growth rate of these layers was set to 1.2, which allows for a smooth transition from the wall to the outer flow region, optimizing the accuracy of the simulation. The y+ values in the wall region were maintained within the recommended range for the SST model, ensuring that the turbulence model operates effectively in the boundary layer. Specifically, the y+ values were targeted

to be around 1, confirming that the mesh resolution is adequate for capturing the flow characteristics accurately.

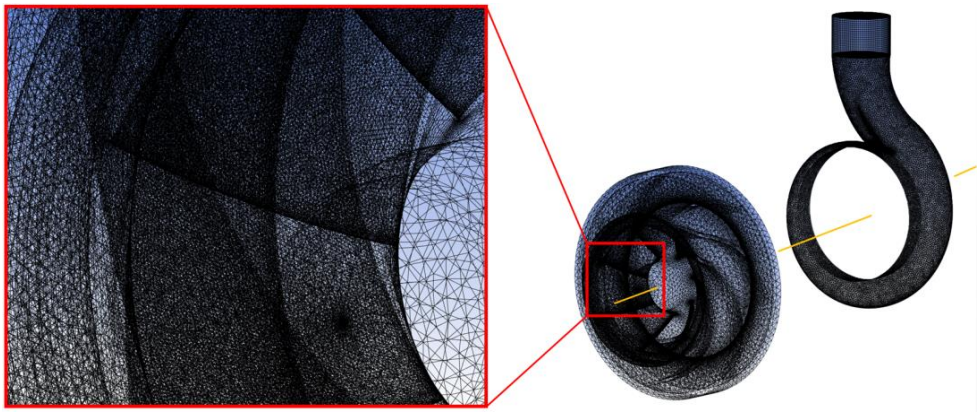

Figure 4. Meshes of the computational domain.

The total number of cells for the impeller, volute, suction, and discharge pipes were 6,368,496, 425,598, 93,852 and 28,640 elements, respectively.

3. Results and Validation of the Developed Models

3.1. Results of the Hydraulic Calculations

Three different hydraulic calculations were performed using the methods of Ivanovsky and Spiridonov, as well as a combined method, which integrates the first two and is supplemented by the consideration of the cavitation coefficient. The results of the calculations, presented in Table 3, were compared with the actual data for the CHP 150-315/1500 pump, provided in the second column of Table 3. According to Ivanovsky's method, the blade width deviations at the LE (b_1) and TE (b_2) were 25% and 43%, respectively. The blade installation angles at the LE also show deviations in the range from 24% to 40%. Spiridonov's method shows a deviation in the outer diameter D_2 by 13% and the blade width at the TE (b_2) by 27.5%. The installation angles of the blade LE at the midsection and at the intersection with the shroud, β_{1b} and β_{1bsh}, deviate by 20% and 38%, respectively. In the combined method proposed by the authors of this article, the deviation in the outer diameter from the actual data is 8.6%, while all other parameters have deviations of less than 7.6%. These results highlight that the cavitation coefficient significantly influences the blade width and angles at both the LE and TE. In the combined method, the cavitation coefficient was set to 0.62. The results demonstrate that the combined method achieves a deviation accuracy of less than 9%, confirming its high precision in comparison to the other methods.

Table 3. Main geometric parameters of the impeller.

Parameters	CHP 150-315/1500	Ivanovsky		Spiridonov		Combined k_{cav} = 0.62	
		Value	Deviation	Value	Deviation	Value	Deviation
D_{sh}, [mm]	46	45.9	0.2%	45.9	0.2%	46.8	1.7%
D_h, [mm]	60	65.0	8.3%	60.6	1.0%	61.8	3.0%
D_0, [mm]	190	187.6	1.3%	188.0	1.1%	187.9	1.1%
D_1, [mm]	132	131.4	0.5%	132.0	0.0%	131.5	0.4%
D_2, [mm]	324	346.0	6.8%	368.0	13.6%	296.1	8.6%
D_{1sh}, [mm]	190	187.6	1.3%	188.0	1.1%	187.9	1.1%
D_{1h}, [mm]	74	75.1	1.5%	76.0	2.7%	75.2	1.6%
b_1, [mm]	80	60.0	25.0%	85.0	6.3%	75.4	5.8%
b_2, [mm]	40	22.8	43.1%	29.0	27.5%	42.0	5.0%
β_{1b}, [°]	20	26.1	30.7%	24.1	20.4%	19.9	0.4%
β_{2b}, [°]	34	34.4	1.3%	37.6	10.4%	34.5	1.6%
β_{1bsh}, [°]	14	19.7	40.4%	19.4	38.4%	15.1	7.6%
β_{1bh}, [°]	32	39.8	24.4%	34.5	7.7%	30.0	6.2%

As a result of the calculations, the overall calculated efficiency was 80%. The efficiency accounting for the bearing friction and the clearance between the impeller and the volute was approximately 92%, while the efficiency considering the seal leakage reached 97%. The hydraulic efficiency of the pump, which is the lowest and takes into account the energy losses due to hydraulic friction, vortices, and flow separation, was 90%.

In this method, the nominal shaft power of the pump was 32.7 kW, while the maximum calculated power reached 37 kW.

3.2. Results of CFD Modeling

To ensure the validity of the hydrodynamic model, numerical simulations of the flow in a single-stage centrifugal pump with single suction were performed under various flow rate conditions, corresponding to the experimental test data. The convergence of the solution was achieved in approximately 600 to 1000 iterations, depending on the flow rate. The comparison between the numerical results and the experimental data for pressure head and efficiency showed strong correlation, as illustrated in Figure 5. The maximum relative error in the pressure head calculations did not exceed 3.9%, while the largest deviation in efficiency was less than 5.4%. These findings demonstrate the reliability of the developed algorithm and its capability to accurately reproduce the real performance characteristics of the pump under the tested conditions.

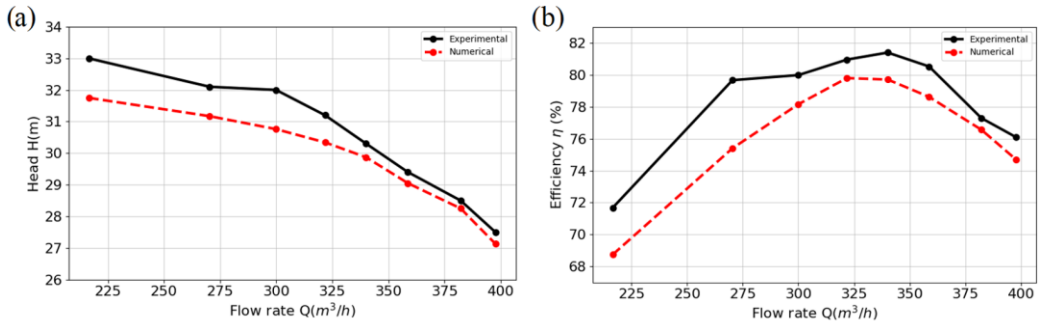

Figure 5. Comparison of the hydraulic performances of the centrifugal pump. (**a**) Head (H)—flow rate (Q); (**b**) efficiency (η)—flow rate (Q).

Figures 6 and 7 show the pressure and velocity distributions inside the impeller and volute casing of a centrifugal pump, obtained as a result of numerical simulation using computational fluid dynamics (CFD) methods, at a flow rate of Q = 300 m^3/h. The pressure distribution reflects the typical dynamics for a centrifugal pump (Figure 6). The inlet pressure is about 0.3 × 10^5 Pa, which corresponds to the specified value of 0.3 atm. Minimum pressure values are observed at the beginning of the impeller blades, reaching −2.75 × 10^5 Pa. In this zone, the liquid begins to interact with the blades, where the centrifugal forces significantly accelerate the flow, which causes a sharp drop in pressure. As the liquid moves from the inlet to the outlet, the pressure in the impeller increases, which is associated with the conversion of the kinetic energy of the flow into potential energy due to the action of the centrifugal forces. In the volute casing, where the flow slows down due to the expanding section, the pressure continues to increase. At the pump outlet, it reaches values of about 3.3 × 10^5 Pa, which indicates the successful operation of the pump in converting the energy of liquid movement into hydraulic pressure.

Figure 7 shows the velocity distribution fields inside the impeller and volute casing of a centrifugal pump, obtained as a result of numerical simulation using the CFD methods. At the center of the pump, where the liquid enters, the flow velocity is low, which is typical for the initial conditions when the liquid has not yet been affected by the blades. As the liquid enters the impeller, the velocity begins to increase under the action of the centrifugal forces and reaches its maximum at the periphery of the blades. In the volute, the velocity gradually decreases, facilitating the conversion of the kinetic energy of the flow into static pressure. Also observed are zones with reduced velocity on the upper parts of the blades,

which may indicate localized areas of turbulence or uneven flow. These features illustrate the complex interaction of the flow with the impeller blades and volute casing, ensuring the efficient operation of the pump.

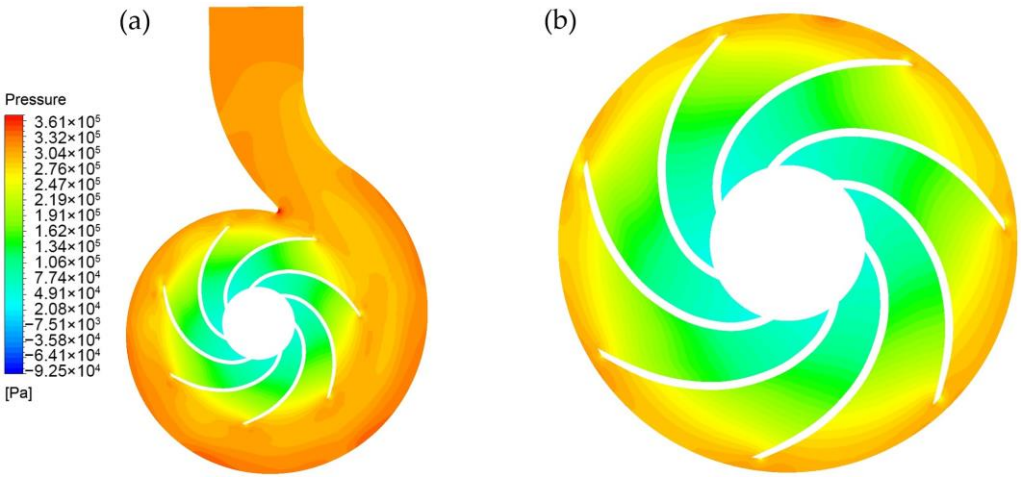

Figure 6. Pressure contour distribution in the radial cross section of a pump (**a**) and impeller (**b**).

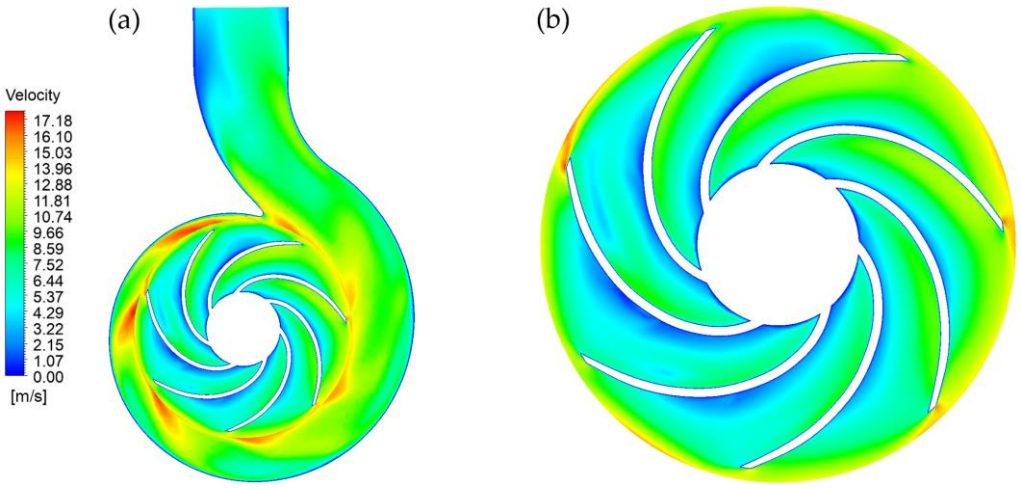

Figure 7. Velocity contour distribution in the radial cross section of a pump (**a**) and impeller (**b**).

4. Parametric Study

The impeller is a key element of a centrifugal pump, responsible for converting the mechanical rotational energy into the kinetic and potential energy of the fluid flow. For a detailed analysis of its operation, hydrodynamic modeling of a single blade sector, without taking into account the volute, was conducted at a flow rate of Q = 300 m^3/h and a rotation speed of n = 1500 rpm. The modeling results showed that the pressure created by the impeller was H = 36.9 m, and the efficiency coefficient (EC) reached η = 95.7%. These data confirm the high efficiency of the impeller under the specified conditions, which indicates the correct design and optimal hydrodynamic characteristics.

Then, a parametric analysis of the impeller was carried out, during which the geometric parameters of the blades were varied (see Table 4), including the blade LE angles (β_{1b}, β_{1bsh}, β_{1bh}), blade TE angle (β_{2b}), blade wrap angles (φ, φ_{sh}, φ_h), and the TE shape (Figure 8). The analysis is aimed at assessing the influence of these parameters on the hydraulic characteristics, such as the pressure and efficiency. The initial parameters of the impeller were set as follows: blade LE angle β_{1b} = 20°, β_{1bsh} = 14°, β_{1bh} = 32°; blade TE angle β_{2b} = 34°; blade wrap angles φ_{sh} = 112.2°, φ_h = 127°, φ = 119.2°; the TE shape was defined as “Simple”. Changing these parameters allows for a deeper understanding of

their impact on the pump performance and the identification of the optimal values for achieving high performance and efficiency.

Table 4. Blade profiles under consideration.

Parameters	Values					
blade LE angles	$\beta_{1b} = 14°$ $\beta_{1bsh} = 8°$ $\beta_{1bh} = 26°$	$\beta_{1b} = 16°$ $\beta_{1bsh} = 10°$ $\beta_{1bh} = 28°$	$\beta_{1b} = 18°$ $\beta_{1bsh} = 12°$ $\beta_{1bh} = 30°$	$\beta_{1b} = 22°$ $\beta_{1bsh} = 16°$ $\beta_{1bh} = 34°$	$\beta_{1b} = 24°$ $\beta_{1bsh} = 18°$ $\beta_{1bh} = 36°$	$\beta_{1b} = 26°$ $\beta_{1bsh} = 20°$ $\beta_{1bh} = 38°$
blade TE angle	$\beta_{2b} = 28°$	$\beta_{2b} = 30°$	$\beta_{2b} = 32°$	$\beta_{2b} = 36°$	$\beta_{2b} = 38°$	$\beta_{2b} = 40°$
blade wrap angles	$\varphi_{sh} = 106.2°$ $\varphi_h = 121.0°$ $\varphi = 113.2$	$\varphi_{sh} = 108.2°$ $\varphi_h = 123.0°$ $\varphi = 115.2°$	$\varphi_{sh} = 110.2°$ $\varphi_h = 125.0°$ $\varphi = 117.2°$	$\varphi_{sh} = 114.2°$ $\varphi_h = 129.0°$ $\varphi = 121.2°$	$\varphi_{sh} = 116.2°$ $\varphi_h = 131.0°$ $\varphi = 123.2°$	$\varphi_{sh} = 118.2°$ $\varphi_h = 133.0°$ $\varphi = 125.2°$

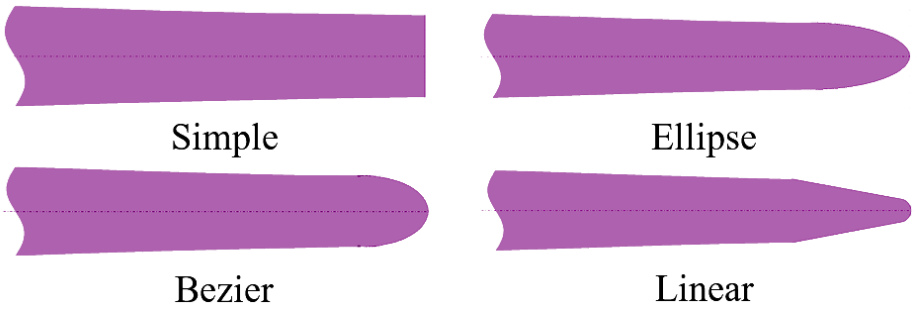

Figure 8. Shapes of blade trailing edge.

Figures 9 and 10 show the results of the parametric analysis of the impeller. The next section analyzes the influence of each parameter on the hydraulic characteristics of the impeller. The influence of the blade LE angles, TE angle, and blade wrap angles are shown in Figure 9. Changing the blade LE angles did not have a significant effect on the pressure head but had a significant effect on the efficiency. When the angles were reduced by 6°, the efficiency increased by 0.31%, while when they were increased by 6°, it decreased by 0.57%. The blade TE angle had a significant effect on the pressure head: when the angle was increased by 6°, the pressure head increased by 1.24 m, and the efficiency increased by 0.23%. When the angle was reduced by 6°, the pressure head decreased by 1.61 m, and the efficiency decreased by 1.04%. Increasing the wrap angles had an insignificant effect on the pressure head and efficiency. However, with a 6° reduction in angles, the head and efficiency decreased by 0.81 m and 0.6%, respectively.

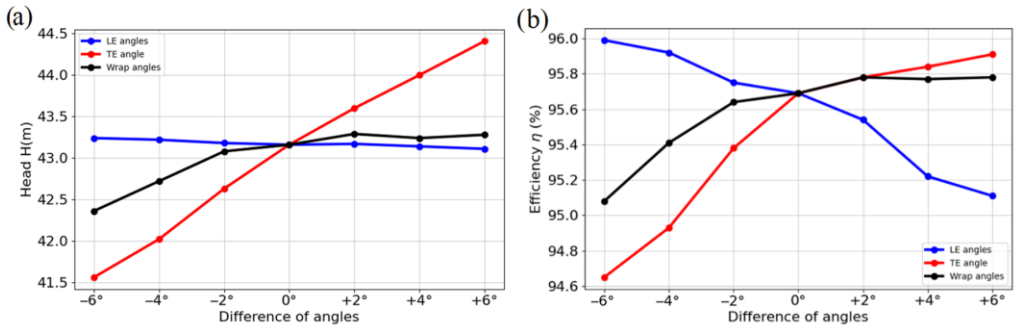

Figure 9. Comparison of the hydraulic performances of the impeller. (**a**) Head (H)—difference in angles; (**b**) efficiency (η)—difference in angles.

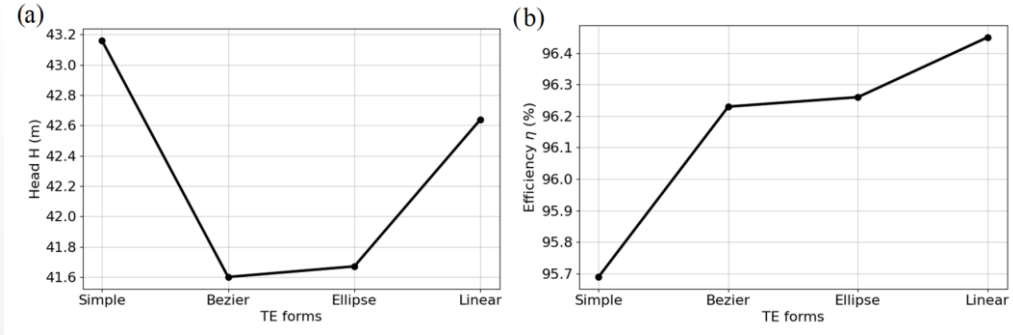

Figure 10. Comparison of the hydraulic performances of impeller. (**a**) Head (H)—TE form; (**b**) efficiency (η)—TE form.

Figure 10 analyzes the influence of the blade TE shape on the impeller hydraulic characteristics. Three alternative shapes were considered: ellipse, Bezier, and linear. All the new shapes demonstrated a lower pressure compared to the original shape (simple). The maximum pressure drop of 1.57 m was recorded for the ellipse shape, while the minimum drop of 0.53 m was observed for the linear shape. Despite this, the efficiency of all three shapes was higher than the original, with the linear shape demonstrating the greatest increase in efficiency by 0.76%.

Figure 11 shows the blade loadings at 20%, 50%, and 80% span. In each case, despite the blade profile changes, there is a tendency for the pressure to increase from an initial value of 0.3×10^5 Pa (0.3 atm) at the inlet to more than 3×10^5 Pa at the blade tip.

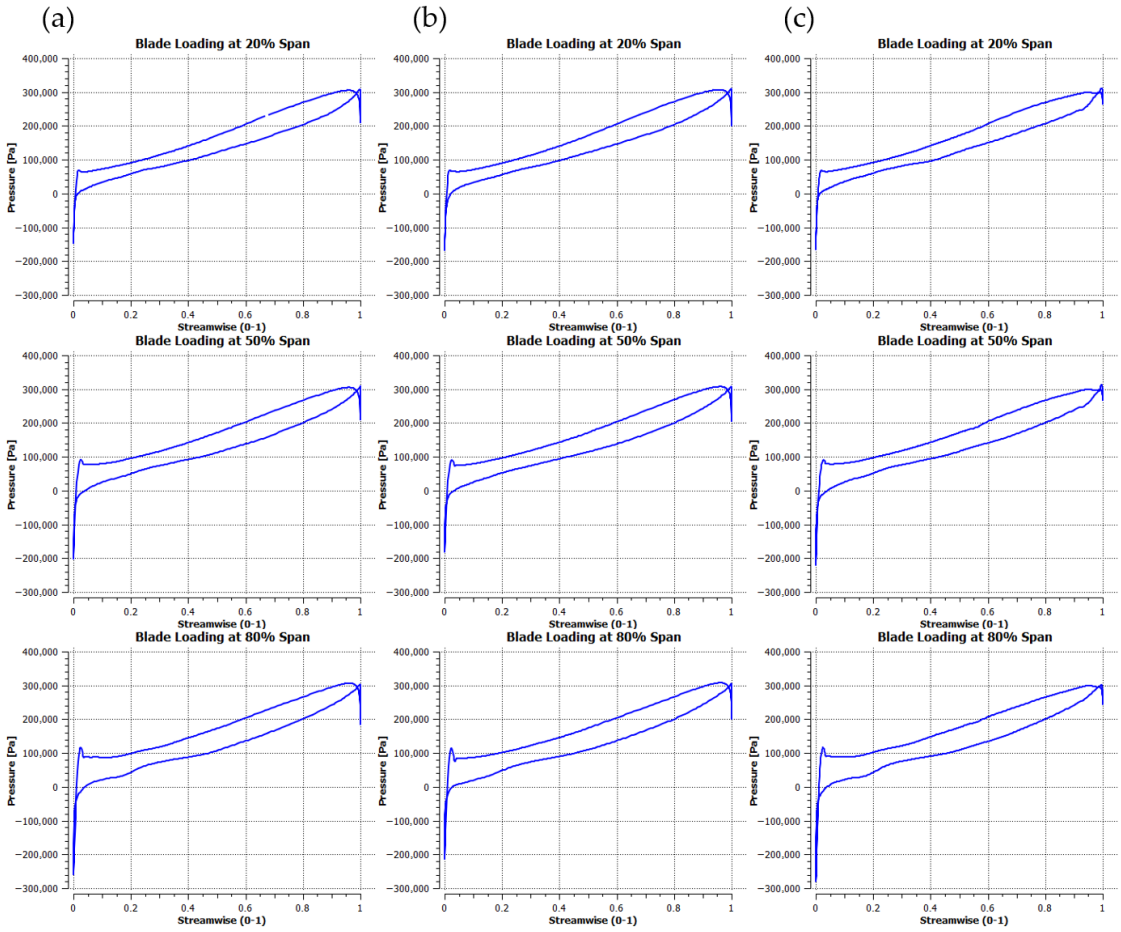

Figure 11. Blade loadings. (**a**) Original impeller; (**b**) β_{1b} = 14°, β_{1bsh} = 8°, β_{1bh} = 16°; (**c**) linear TE form.

A significant pressure drop is recorded at the leading edge of the blade. For the original impeller, these drops are −148,065 Pa, −204,238 Pa, and −261,739 Pa at 20%, 50%, and 80% of the hub, respectively (Figure 11a). This phenomenon is due to the increase in the fluid velocity caused by acceleration near the blade inlet. The minimum pressure drop values of −168,964 Pa, −182,457 Pa, and −214,801 Pa were recorded at the leading edge at the inlet angles β_{1b} = 14°, β_{1bsh} = 8°, and β_{1bh} = 16° (Figure 11b).

A pressure drop of up to 2 × 10^5 Pa is also observed at the trailing edge, which is associated with the formation of a flow separation zone and local liquid recirculation. Changing the shape of the blade trailing edge resulted in a reduction in the pressure drop at the blade exit, which contributed to flow stabilization at the outlet (Figure 11c).

In other cases, the pressure changes at the leading and trailing edges were either lower or similar to the values obtained for the original impeller.

Based on the conducted studies, the optimal impeller should have the following parameters: reduced blade inlet angles ($\beta_{1b} = 14°$, $\beta_{1bsh} = 8°$, $\beta_{1bh} = 26°$), increased blade outlet angle ($\beta_{2b} = 40°$), original wrap angles ($\varphi = 119.2°$, $\varphi_{sh} = 112.2°$, $\varphi_h = 127°$), and linear trailing edge shape. These optimal values will improve the hydraulic performance of the impeller, resulting in enhanced efficiency and head.

5. Conclusions

As a result of the hydraulic calculations performed using the methods of Ivanovsky, Spiridonov, and a combined method that considers the cavitation coefficient, the following results were obtained. Ivanovsky's method demonstrated deviations in the blade width at the LE and TE of 25% and 43%, respectively. In contrast, Spiridonov's method revealed a deviation of 13% in the outer diameter D_2 and 27.5% in the blade width at the TE. Meanwhile, the combined method proposed by the authors achieved a deviation in the outer diameter of only 8.6% and deviations in other parameters of less than 7.6%. These results underscore the significant influence of the cavitation coefficient on both the width of the blades and the installation angles at the LE and TE. The combined method demonstrated high calculation accuracy, with a deviation of less than 9% compared to the other methods.

Additionally, a hydrodynamic model was developed, enabling a detailed study of the hydrodynamic processes within the pump. A verification calculation was performed using experimental data, revealing that the maximum relative error in the calculated head was 3.9%, while the deviation in efficiency was less than 5.4%. These findings confirm the reliability of the proposed algorithm.

During the conducted parametric analysis, two key parameters were identified as significantly affecting the pump's efficiency coefficient. First, the angle of the blade's trailing edge has a substantial impact on the pump characteristics; a change of 6° in this angle significantly influences both the head and efficiency, increasing them when the angle is increased and vice versa. Second, the shape of the trailing edge also plays a critical role, as transitioning to a linear form enhances efficiency, albeit at the cost of a reduced head. These results highlight the necessity of optimizing the geometric parameters of the blades to improve the performance of the centrifugal pump.

Author Contributions: Conceptualization, N.J. and A.K.; Methodology, A.A., T.A., A.S., N.M., N.J. and A.K.; Software, A.A. and A.S.; Validation, A.A., T.A., A.S. and N.M.; Formal analysis, N.J. and A.K.; Investigation, A.A., T.A., A.S. and N.M.; Writing—original draft, T.A.; Supervision, A.K. All authors have read and agreed to the published version of the manuscript.

Funding: The authors express their deep gratitude for the financial support received through the Research Grant from the Ministry of Science and Higher Education of the Republic of Kazakhstan (Grant Number: BR18574035).

Data Availability Statement: The original contributions presented in the study are included in the article, further inquiries can be directed to the corresponding author.

Acknowledgments: The authors would like to express their gratitude to the Karlskrona LC AB manufacturing plant (Shymkent, Kazakhstan) for their collaboration in the study and for providing the necessary data on the CHP 150-315/1500 pump.

Conflicts of Interest: The authors declare no conflict of interest.

References

1. Jianxin, H.; Li, K.; Su, W.; Zhao, X. Numerical Simulation of Drilling Fluid Flow in Centrifugal Pumps. *Water* **2023**, *15*, 992. [CrossRef]
2. Bellary, S.A.I.; Samad, A. Pumping crude oil by centrifugal impeller having different blade angles and surface roughness. *J. Pet. Explor. Prod. Technol.* **2016**, *6*, 117–127. [CrossRef]
3. Kim, B.; Siddique, M.H.; Samad, A.; Hu, G.; Lee, D.-E. Optimization of centrifugal pump impeller for pumping viscous fluids using direct design optimization technique. *Machines* **2022**, *10*, 774. [CrossRef]
4. Chang, G.; Gao, M.; He, S. A Review of the Flow-Induced Noise Study for Centrifugal Pumps. *Appl. Sci.* **2020**, *10*, 1022. [CrossRef]
5. Shankar, V.K.A.; Umashankar, S.; Paramasivam, S.; Hanigovszki, N. A comprehensive review on energy efficiency enhancement initiatives in centrifugal pumping system. *Appl. Energy* **2016**, *181*, 495–513. [CrossRef]
6. Noon, A.A.; Kim, M.-H. Erosion wear on centrifugal pump casing due to slurry flow. *Wear* **2016**, *364-365*, 103–111. [CrossRef]
7. Song, X.; Liu, C. Experimental study of the floor-attached vortices in pump sump using V3V. *Renew. Energy* **2021**, *164*, 752–766. [CrossRef]
8. Sorguven, E.; Incir, S.; Highgate, J. Understanding loss generation mechanisms in a centrifugal pump using large eddy simulation. *Int. J. Heat. Fluid. Flow.* **2022**, *96*, 108994. [CrossRef]
9. Chen, B.; Yu, L.; Li, X.; Zhu, Z. Insights into turbulent flow structure and energy dissipation in centrifugal pumps: A study utilizing time-resolved particle image velocimetry and proper orthogonal decomposition. *Ocean. Eng.* **2024**, *304*, 117903. [CrossRef]
10. Cao, W.; Jia, Z.; Zhang, Q. Near-Wall Flow Characteristics of a Centrifugal Impeller with Low Specific Speed. *Processes* **2019**, *7*, 514. [CrossRef]
11. Dehghan, A.A.; Shojaeefard, M.H.; Roshanaei, M. Exploring a new criterion to determine the onset of cavitation in centrifugal pumps from energy-saving standpoint; experimental and numerical investigation. *Energy* **2024**, *293*, 130681. [CrossRef]
12. Fu, Y.; Yuan, J.; Yuan, S.; Pace, G.; D'Agostino, L.; Huang, P.; Li, X. Numerical and Experimental Analysis of Flow Phenomena in a Centrifugal Pump Operating Under Low Flow Rates. *J. Fluids Eng.* **2015**, *137*, 011102. [CrossRef]
13. Deng, S.-S.; Li, G.-D.; Guan, J.-F.; Chen, X.-C.; Liu, L.-X. Numerical study of cavitation in centrifugal pump conveying different liquid materials. *Results Phys.* **2019**, *12*, 1834–1839. [CrossRef]
14. Han, X.; Kang, Y.; Li, D.; Zhao, W. Impeller Optimized Design of the Centrifugal Pump: A Numerical and Experimental Investigation. *Energies* **2018**, *11*, 1444. [CrossRef]
15. Wheeler, A.P.S.; Sofia, A.; Miller, R.J. The effect of leading-edge geometry on wake interactions in compressors. In Proceedings of the ASME Turbo Expo. 2007: Power for Land, Sea, and Air, Montreal, QC, Canada, 14–17 May 2007; pp. 1769–1779. [CrossRef]
16. Luo, H.; Tao, R.; Yang, J.; Wang, Z. Influence of Blade Leading-Edge Shape on Rotating-Stalled Flow Characteristics in a Centrifugal Pump Impeller. *Appl. Sci.* **2020**, *10*, 5635. [CrossRef]
17. Li, H.; Chen, Y.; Yang, Y.; Wang, S.; Bai, L.; Zhou, L. CFD Simulation of Centrifugal Pump with Different Impeller Blade Trailing Edges. *Mar. Sci. Eng.* **2023**, *11*, 402. [CrossRef]
18. Litfin, O.; Delgado, A.; Haddad, K.; Klein, H. Numerical and experimental investigation of trailing edge modifications of centrifugal wastewater pump impellers. In Proceedings of the ASME Fluids Engineering Division Summer Meeting, Waikoloa, HI, USA, 30 July–3 August 2017; p. V01AT05A008. [CrossRef]
19. Xu, Z.; Kong, F.; Tang, L.; Liu, M.; Wang, J.; Qiu, N. Effect of Blade Thickness on Internal Flow and Performance of a Plastic Centrifugal Pump. *Machines* **2022**, *10*, 61. [CrossRef]
20. Yang, S.S.; Wang, C.; Chen, K.; Yuan, X. Research on Blade Thickness Influencing Pump as Turbine. *Adv. Mech. Eng.* **2014**, *6*, 190530. [CrossRef]
21. Tao, Y.; Yuan, S.; Liu, J.; Zhang, F.; Tao, J. The influence of the blade thickness on the pressure pulsations in a ceramic centrifugal slurry pump with annular volute. *Proc. Inst. Mech. Eng. Part A: J. Power Energy* **2017**, *231*, 415–431. [CrossRef]
22. Gülich, J.F. Pump Hydraulics and Physical Concepts. In *Centrifugal Pumps*, 3rd ed.; Springer: Villeneuve, Switzerland, 2014; pp. 79–156. [CrossRef]
23. Chinyaev, I.A. *Blade Pumps [Lopastnye Nasosy]*; Voronov, V.F., Ed.; Leningrad Mashinostroenie: Leningrad, USSR, 1973; p. 185. (In Russian)
24. Ivanovsky, V.N.; Sabirov, A.A.; Degovtsov, A.V.; Donskoy, Y.A.; Pekin, S.S.; Krivenkov, S.V.; Sokolov, N.N.; Kuzmin, A.V. *Design and Study of Dynamic Pump Stages [Proektirovanie i Issledovanie Stupeney Dinamicheskikh Nasosov]*; Gubkin Russian State University of Oil and Gas: Moscow, Russia, 2014; p. 124. (In Russian)
25. Spiridonov, E.K.; Prokhasko, L.S. *Calculation and Design of Blade Pumps: A Textbook [Raschet i Proektirovanie Lopastnykh Nasosov: Uchebnoe Posobie]*; South Ural State University: Chelyabinsk, Russia, 2004; p. 62. (In Russian)

26. Gorgidzhanyan, S.A. *Hydraulic Calculations of the Flow Path of Centrifugal Pumps: Methodological Guidelines for Course Design [Gidravlicheskie Raschety Protochnoy Chasti Tsentrifugalnykh Nasosov: Metodicheskie Ukazaniya po Kursovomu Proektirovaniyu]*; Martynova, S.A., Ed.; Kalinin Leningrad Polytechnic Institute: Leningrad, USSR, 1982. (In Russian)
27. Mikhailov, A.K.; Malyushenko, V.V. *Blade Pumps: Theory, Calculation, and Design [Lopastnye Nasosy. Teoriya, Raschet i Konstruirovanie]*; Yakunina, I.I., Ed.; Moscow Mashinostroenie: Moscow, Russia, 1977; p. 304. (In Russian)
28. Lomakin, A.A. *Centrifugal and Axial Pumps [Tsentrifugalnye i Osevyye Nasosy]*; Vasileva, V.P., Orlova, L.I., Eds.; Leningrad Mashinostroenie: Leningrad, USSR, 1965; p. 364. (In Russian)
29. Menter, F.R. Zonal Two Equation k-ω Turbulence Models for Aerodynamic Flows. In Proceedings of the 24th Fluid Dynamics Conference, Orlando, FL, USA, 6–9 July 1993; p. 2906.
30. Menter, F.R. Two-Equation Eddy-Viscosity Turbulence Models for Engineering Applications. In Proceedings of the AIAA 23rd Fluid Dynamics, Plasmadynamics, and Lasers Conference, Orlando, FL, USA, 6–9 July 1993; pp. 1598–1605.
31. Colli, A.N.; Bisang, J.M. A CFD Study with Analytical and Experimental Validation of Laminar and Turbulent Mass-Transfer in Electrochemical Reactors. *J. Electrochem. Soc.* **2018**, *165*, 81–88. [CrossRef]
32. Colli, A.N.; Bisang, J.M. Coupling k Convection-Diffusion and Laplace Equations in an Open-Source CFD Model for Tertiary Current Distribution Calculations. *J. Electrochem. Soc.* **2020**, *167*, 013513. [CrossRef]
33. Rajendran, S.; Purushothaman, K. Analysis of a Centrifugal Pump Impeller Using ANSYS-CFX. *Int. J. Eng. Res. Technol. IJERT* **2012**, *1*, 1–6. Available online: https://www.ijert.org/research/analysis-of-a-centrifugal-pump-impeller-using-ansys-cfx-IJERTV1IS3098.pdf (accessed on 28 October 2024).